Chemical Engineering Journal 165 (2010) 639–648

Contents lists available at ScienceDirect

Chemical Engineering Journal

journal homepage: www.elsevier.com/locate/cej

Multi-objective optimization in solid oxide fuel cell for oxidative coupling of methane

Mohammad R. Quddus, Yan Zhang, Ajay K. Ray*

Department of Chemical and Biochemical Engineering, University of Western Ontario, London, ON N6A 5B9, Canada

ARTICLE INFO

Article history:
Received 18 January 2010
Received in revised form 27 August 2010
Accepted 10 September 2010

Keywords:
Multi-objective optimization
Solid oxide fuel cell
Oxidative coupling of methane
Pareto solutions

ABSTRACT

Multi-objective optimization of a solid oxide fuel cell (SOFC) reactor for oxidative coupling of methane has been studied with the elitist non-dominated sorting genetic algorithm with jumping genes (NSGA-II-aJG). A parametric sensitivity analysis was carried out on the experimentally verified model to systematically investigate the effects of the process parameters on the performance of the SOFC reactor. Several two and three objective optimization problems were performed using NSGA-II-aJG. Significant performance improvement in terms of C_2 yield and electrical power could be achieved when rigorous optimization was performed. These sets of solution narrow down the choices available to a decision maker, who can choose the 'preferred' solution among the points in the set.

1. Introduction

Solid oxide fuel cell (SOFC) is one of the promising technologies that have the potential of simultaneous generation of electrical energy and valuable products. On the other hand, oxidative coupling of methane (OCM) facilitates the formation of valuable C_2 (ethane and ethylene) products by coupling two molecules of methane (CH_4) with less emission of green house gas (CO_2) to the atmosphere. As a consequence OCM is coupled with SOFC as an approach towards the development of a green technology and is thus extensively studied. After the first demonstration in solid oxide membrane reactor by Otsuka and Jinno with Ag or Ag/Bi_2O_3 applied on yttria stabilized zirconia (YSZ) [1], Pujare and Sammells [2] were the first to report spontaneous electrochemical synthesis of C_2 hydrocarbon species and direct electric energy from CH_4 in SOFC. A SOFC consists of an electrolyte material, which is interposed between two thin electrodes (porous anode and cathode). Direct chemical combustion is prevented by the electrolyte (YSZ) that separates the fuel (CH_4) and from oxidant (O_2). The electrolyte serves as a barrier to gas diffusion, but allows migration of ions across it. Gaseous oxygen is selectively activated on cathode catalyst into O^{2-} as lattice oxygen, which is transferred to anode catalyst through YSZ electrolyte. The permeated oxygen is then activated on the anode catalyst to react with methane to form valuable C_2 products [3]. The flow of ionic charge through the electrolyte must be balanced by the flow of electronic charge through an outside circuit, and it is this balance that produces electrical power [4]. Later, several experimental studies were reported focusing the catalyst preparation [5–7], characterization [8] and reactor performance tests [9–14].

Besides the experimental studies, modeling emerged as a comprehensive tool for the design of SOFC and prediction of its performance for OCM. Xui-mei et al. proposed a mathematical model based on well mixed flow and plug flow for OCM in SOFC [15]. Later on Kaitkittipong et al. [8,9,16] reported a well defined plug flow model for a LSM/YSZ/LaAlO reactor. Unfortunately, all these mathematical models are not yet subjected to systematic and rigorous optimization study which could significantly improve the performance of an SOFC.

Therefore, the systematic study of optimization for OCM using SOFC was performed in this work. Moreover, rather than single objective optimization, several systematic investigation of multi-objective optimization (MOO) was carried out in this study, as most real-world chemical engineering problems require the simultaneous optimization of several objectives (multi-objectives) that are non-commensurate. Similarly, the design and operation of SOFC require the minimization or maximization of several objectives which are often conflicting. Therefore, the results of MOO are meant to be more valuable than those of a single objective optimization. Thus rigorous MOO of SOFC reactor is needed. However, before solving any optimization problem, it is a common practice to make sure that the model used for MOO is good enough to predict the experimental data. In this study, the model proposed by Kaitkittipong et al. [8] was used and it was also validated by their experimental data before formulation of any MOO cases. Next, a parametric sensitivity analysis was carried out on the experimentally verified model to systematically investigate the effects of the process parameters on the performance of the SOFC. Thereafter the

* Corresponding author. Tel.: +1 519 661 2111x81279; fax: +1 519 661 3498.
E-mail address: aray@eng.uwo.ca (A.K. Ray).

1385-8947/$ – see front matter © 2010 Published by Elsevier B.V.
doi:10.1016/j.cej.2010.09.041

Nomenclature

A	pre-factor (m^2/(kg Pa))
A_s	area (m^2)
E	cell voltage (V)
E_a	activation energy (J/mol)
E_L	voltage across load (V)
F	Faraday constant (96,485 EC/mol)
F_i	flow rate (mol/s)
I	current (A)
J	permeation flux (mol/(m^2 s))
k	rate constant (m^2/(kg Pa))
l_{substr}	length of sub-string for each decision variables
L	length of the reactor (m)
N_{gen}	number of generations
N_{pop}	number of populations
p	partial pressure (Pa)
p_c	crossover probability
p_{JG}	jumping probability
p_m	mutation probability
P	power (W)
$P_{t,AN}$	total pressure at the anode side (Pa)
$P_{O_2,CA}$	total pressure at the cathode side (Pa)
r	rate of reaction (mol/(kg s))
R	gas constant (8.314 J/(mol K))
R_{int}	internal resistance (Ω)
R_L	load resistance (Ω)
S_{C_2}	selectivity of C_2 products
S_r	seed for random number generator
T	temperature (K)
W_{cat}	catalyst weight (kg)
x	dimensionless axial length divided by total length of the reactor
X_{CH_4}	conversion of methane
y	mole fraction
z	axial length (m)

Greek symbols

φ	surface concentration (mol/m^2)
γ	flow ratio ($F_i/F^0_{CH_4}$)

Subscripts

AN	anode
C_2	C_2H_6 and C_2H_4
CA	cathode
CO_x	CO and CO_2
cou	coupling site
i	component or reaction *i*
j	oxygenate or coupling site
oxy	oxygenate site

Superscript

0	feed condition

model was interfaced with a state-of-the-art AI based robust non-traditional global optimization technique, non-dominated sorted genetic algorithm [17,18] to perform systematic multi-objective optimization study.

2. Modeling and validation

The mathematical model developed by Kiatkittipon et al. [8] was for SOFC with shell and tube type arrangement. A tube-type membrane consisting of 8 mol% Y_2O_3-ZrO_2 (YSZ) was used as an electrolyte with anode catalyst, $La_{1.8}Al_{0.2}O_3$ (LaAlO) on the inner surface of the tube while the cathode, $La_{0.85}Sr_{0.15}MnO_3$ (LSM) was on the outer side of tube. Methane was fed to the anode at 4.63 cm^3/min while 13.9 cm^3/min of oxygen was fed to the cathode. No dilution was used for the feed gas. The experiment was reported to be performed at three different operation temperatures, 1173, 1223 and 1273 K. The permeation of oxygen was controlled using the resistance box where resistance was varied from 0 to 15 Ω. The total pressure of both the shell and tube side of the cell was maintained same for avoiding cell damage and was 1.013×10^5 Pa. A simplified diagram is shown in Fig. 1, whereas details of the reactor configuration will be found elsewhere [8].

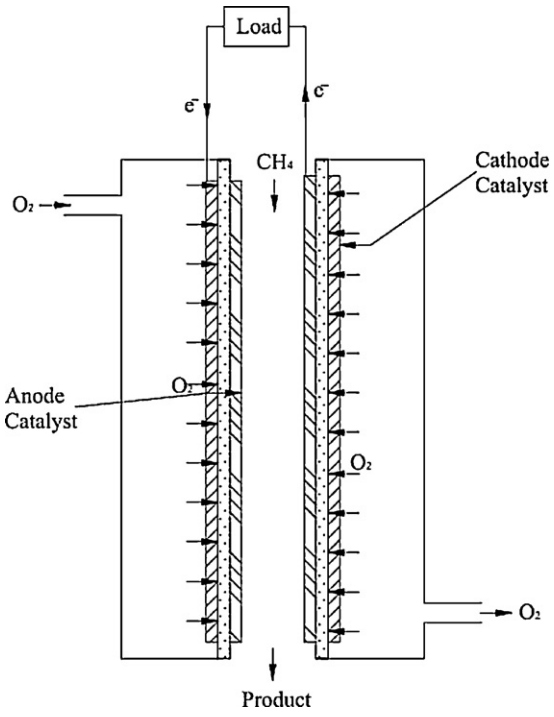

Fig. 1. Simplified diagram of SOFC.

The model was based on the assumption of plug flow. It was also based on the isothermal condition as no significant variation of temperature was observed along the reactor length during the experiments. However, temperature (T) has a significant effect on the characteristics of the anode catalyst. LaAlO was found active for CO and CO_2 formation (oxygenate site) at low temperature (below 1000 K) whereas for C_2 formation (coupling site) it showed higher activity at higher temperature (above 1000 K). The fraction of oxygenate and coupling sites were measured by temperature program desorption (TPD) analysis [9] and was reported in Table 1. Thus based on these assumptions and experimental results the mathematical model they proposed are summarized in Appendix A

All the design equations for SOFC were solved in succession using Compaq Visual Fortran 6.6. Ordinary differential equations were solved numerically with Gear's BDF method, using the DIVPAG subroutine of the IMSL library (Microsoft). Table 2 presents the

Table 1
Mole fraction of oxygen species for the oxygenate and coupling site [8].

	Temperature (K)		
	1173	1223	1273
$y_{O_2,oxy}$	0.490	0.319	0.235
$y_{O_2,cou}$	0.510	0.681	0.765

Table 2
Parameters used in the simulation.

Parameter	Dimensions/range
$F^0_{CH_4}$ (cm^3/min)	4.63
$F^0_{O_2}$ (cm^3/min)	13.9
ID of the membrane (cm)	1.8
A_s (cm^2)	148
W_{cat} (g)	0.04
$P_{O_2,CA}$ (Pa)	1.013×10^5
$P_{t,AN}$ (Pa)	1.013×10^5
R_L (Ω)	0–15
T (K)	1173–1273

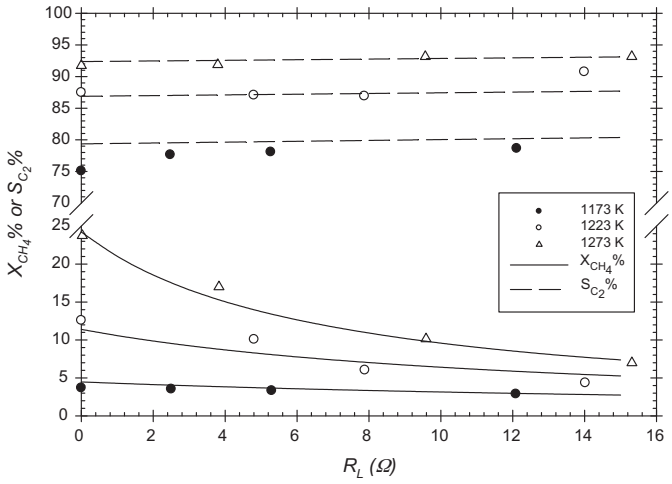

Fig. 2. Comparison of experimental and simulation results.

values of the design and operating parameters used for the reactor simulation.

To validate the model, conversion of methane (X_{CH_4}) and selectivity of C_2 products (S_{C_2}) are compared with the reported experimental results [8] as shown in Fig. 2. It can be concluded that the model resulted in quite good prediction of the experimental conversion and selectivity values with the variation of load resistance (R_L). Increasing temperature had a great influence on the formation of both the C_2 and, CO and CO_2 products. The rate of formation increased with increasing temperature. As a consequence, X_{CH_4} increased with the rise in temperature. But rather than decreasing, increasing trend of S_{C_2} contradicted the influence of temperature on the formation of CO and CO_2 products. This was due to the intrinsic selectivity of the catalyst towards the C_2 products which enhanced with the increase of temperature. As a result the concentration of coupling site increased accompanied by a decrease in the oxygenate site. So the formation of CO and CO_2 actually decreased with the increasing temperature and resulted in an increasing trend of S_{C_2}. Moreover, an increase in the R_L prevented the permeation of oxygen due to an increasing electron transfer resistance. Therefore, a decline in X_{CH_4} was obvious with the increasing R_L. On the other hand, the influence of R_L on selectivity was not that much prominent. This could be again explained by the fact of inherent selectivity of the YSZ membrane electrolyte and parallel formation of coupling and oxygenate sites at a particular T. In addition, the controlled flow of oxygen was liable for the slight increase of S_{C_2} at high value of R_L.

3. Multi-objective optimization

All the multi-objective problems were formulated in such a way that the objectives were independent of time and location, i.e., the objectives increase the scope of making profit rather than maximizing profit itself. So for this study, the most relevant and meaningful objectives are to maximize the C_2 production (F_{C_2}) and minimize the production of undesired side products, CO_x(F_{CO_x}). In addition, recent hike in the demand of fossil fuel more as a raw material of other valuable product synthesis and growing attention to reduce the atmospheric pollution and greenhouse effect influenced the selection of the objectives significantly. Apart from this, SOFC is most attractive to researcher due to its concurrent generation of electrical power and valuable products. So maximization of power (P) at minimum emission of green house gases is a problem of

Table 3
Results of sensitivity analysis and reference values used in the calculation.

	R_L (Ω)		$F^0_{CH_4}$ (cm^3/min)		W_{cat} (g)		T (K)	
	3.79[a]		4.63[a]		0.04[a]		1273[a]	
	−10%[b]	10%[b]	−10%[b]	10%[b]	−10%[b]	10%[b]	−0.50%[b]	0.50%[b]
$F_{C_2H_6}$	−0.69	0.64	−11.58	11.61	1.62	−1.58	−3.73	3.13
$F_{C_2H_4}$	4.11	−3.81	−0.58	0.35	−9.66	9.43	−11.03	14.84
F_{C_2}	3.77	−3.50	−1.34	1.13	−8.88	8.67	−10.53	14.03
X_{CH_4}	3.79	−3.52	9.68	−8.10	−8.92	8.72	−9.96	13.34
S_{C_2}	−0.02	0.02	−0.05	0.05	0.05	−0.04	−0.63	0.60
F_{CO_x}	4.02	−3.73	−0.79	0.57	−9.44	9.23	−2.20	4.11
P	−2.05	1.43	0.00	0.00	0.00	0.00	−4.79	3.62

[a] Reference.
[b] %Change.

Table 4
Formulation of optimization problems solved in this study.

Problem no.	Objective function	Decision variables	Fixed variables	Constraints
Case 1	Max F_{C_2} Min F_{CO_x}	$1160 \le T \le 1287$ K $0.0 \le R_L \le 15.0$ Ω	$P_{t,AN} = 1.013 \times 10^5$ Pa	No Constraints
Case 2	Max P Min F_{CO_x}	$245 \le F^0_{CH_4} \le 575$ cm^3/hr $0.01 \le W_{cat} \le 0.05$ gm	$P_{t,AN} = 1.013 \times 10^5$ Pa $A_s = 148$ cm^2	$X_{CH_4} > 10\%$
Case 3	Max P Max F_{C_2}			No Constraints
Case 4	Max P Max F_{C_2} Min F_{CO_x}			$X_{CH_4} > 10\%$

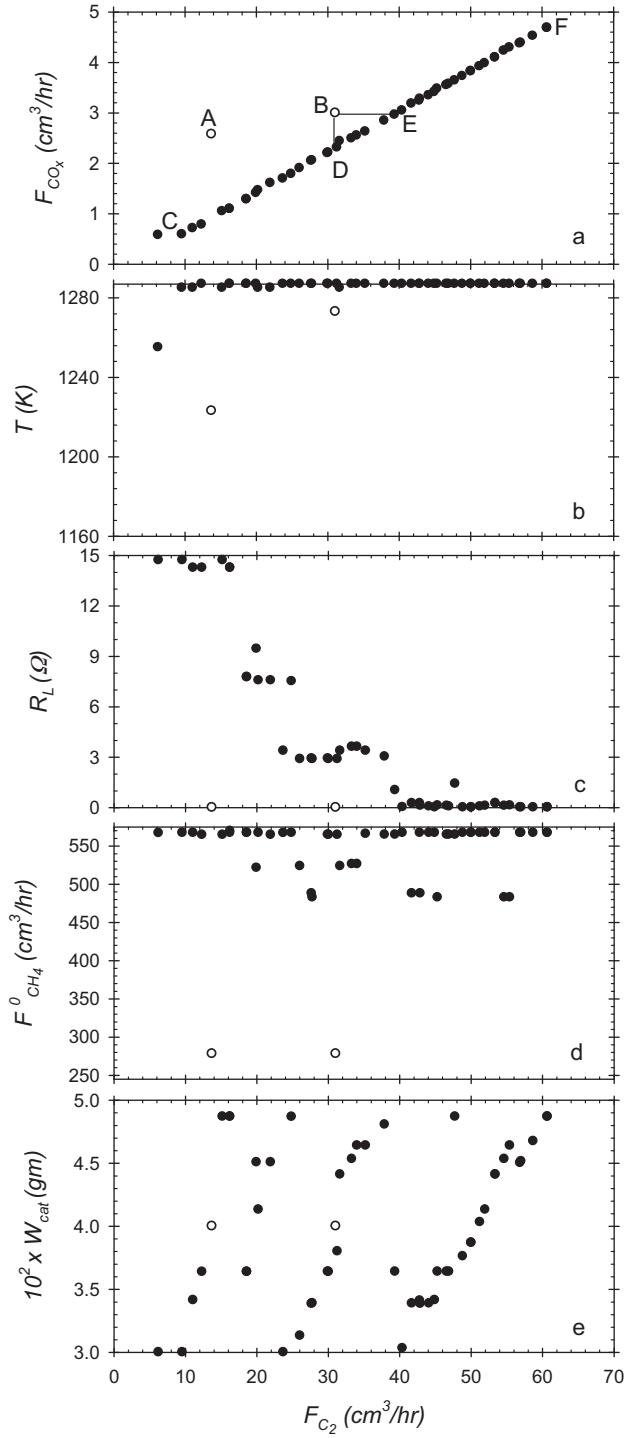

Fig. 3. Results for two-objective optimization: maximization of F_{C_2} and minimization of F_{CO_x}: (a) Pareto-optimal set; (b and c) values of decision variables corresponding to the points of Pareto-optimal set shown in part (a); (○) current experimental operating points.

great interest. Therefore, a systematic multi-objective optimization study was performed to determine the optimal operating conditions and design configurations of the SOFC unit.

3.1. Sensitivity analysis

Sensitivity analysis is one of the key tools used to understand the effect of various parameters on the several performance indicators. This ultimately helps to formulate the multi-objective optimization

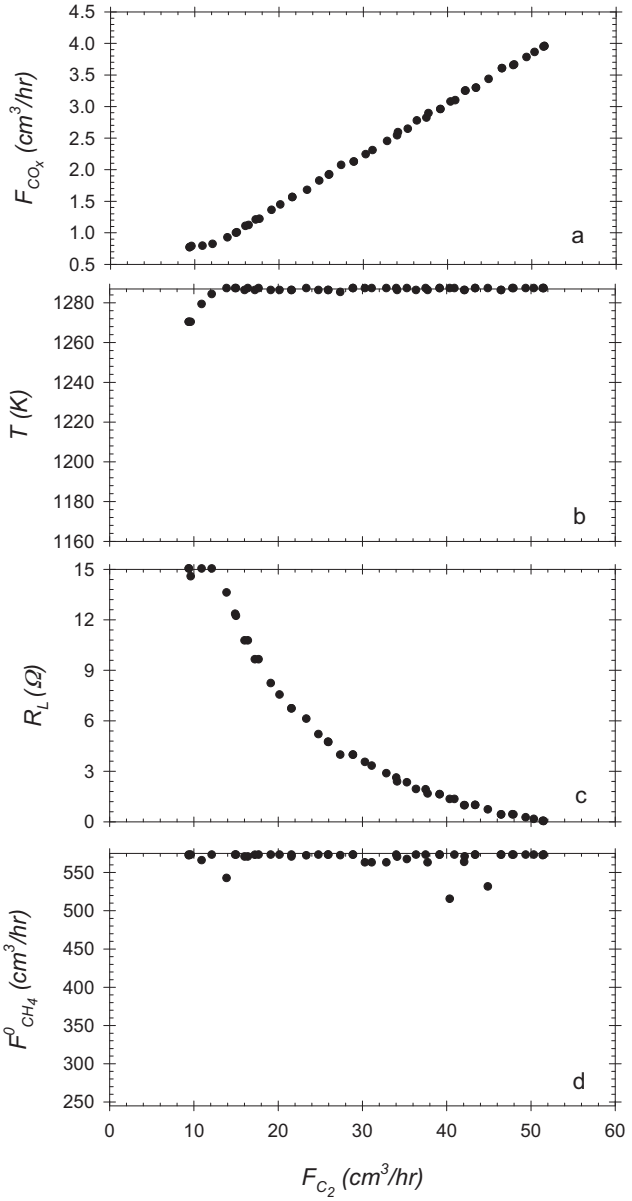

Fig. 4. Results for two-objective optimization: maximization of F_{C_2} and minimization of F_{CO_x} with $W_{cat} = 0.05$ g: (a) Pareto-optimal set; (b–d) values of decision variables corresponding to the points of Pareto-optimal set in part (a).

problems of the system appropriately. Therefore, a sensitivity analysis was performed with the SOFC model by varying one variable at a time around a reference set of values and noting its effect on several performance indicators of the SOFC unit. The effect of operating parameters, such as $F^0_{CH_4}$ (feed flow of CH_4), R_L and T, and one design parameter, W_{cat} (catalyst weight) of the reactor on several performance indicating parameters were studied. The values of each of these variables (except T) were varied within a ±10% of the reference values one at a time keeping the others constant. T was varied ±0.5% of its reference value. The complete results of the analysis are listed in Table 3.

In Table 3, F_{C_2} is the total flow of C_2H_6 and C_2H_4, and F_{CO_x} is for total flow of CO and CO_2. The sensitivity analysis of R_L on the performance parameters showed great influence except for S_{C_2} and $F_{C_2H_6}$. The increase in R_L resulted in a decrease in the permeation of oxygen due to an increasing electron transfer resistance. Thus, the X_{CH_4} decreased with an insignificant increase in the S_{C_2}. Though there was an increase in $F_{C_2H_6}$, a larger decrease in $F_{C_2H_4}$ resulted in

an overall decrease in F_{C_2}. This was also accompanied by a decrease in F_{CO_x} due to parallel formation of oxygenate and coupling sites at the same temperature. A detail discussion about parallel formation had already been presented in Section 2.

Increase in $F^0_{CH_4}$ was accompanied by a decrease in X_{CH_4} due to less residence time in the reactor. Apart from $F_{C_2H_6}$, $F^0_{CH_4}$ did not have an apparent influence on other performance parameters. This substantial increase in $F_{C_2H_6}$ was due to both the kinetics reported in Eqs. (A1)–(A5) and residence time. Thermodynamically, the formation of C_2H_6 requires less activation energy than C_2H_4. And due to less residence time the exposure of the reactant to the catalyst surface was also less. As a result the possible conversion of C_2H_6 to C_2H_4 was impeded. Though the formation of C_2H_6 was much higher in this case it was not substantial enough to have a significant effect on the total C_2 flow rate. Because the formation of C_2H_6 was very small compared to C_2H_4 due to inherent selectivity of the catalyst. As a consequence, there was slight increase in F_{C_2} with the increasing $F^0_{CH_4}$.

It was envisaged that the change in W_{cat} could significantly affect the performance parameter as increased W_{cat} offered more coupling and oxygenate site over the reference point. This was easily perceptible from the sensitivity analysis where increased W_{cat} led to higher X_{CH_4} as well as more formation of C_2 products. In addition F_{CO_x} was also enhanced due to parallel formation of both oxygenate and coupling site. Thus, there was slight change in S_{C_2}. Moreover, there was no effect on the P for both $F^0_{CH_4}$ and W_{cat} as P was not even related to these parameters.

T was found to be the most sensitive parameter from the sensitive analysis. Slight changes in T influenced all the performance parameter significantly. As the temperature was increased not only all the product formation enhanced but also was accompanied by a greater increase in X_{CH_4}. Though the change in selectivity was insignificant it was obvious that the T had the largest influence on generation of the values for selectivity.

3.2. Formulation of multi-objective optimization

It has been proven from the sensitivity analysis that decision variables have the conflicting influence on the performance parameters, and it is not possible to maximize the conversion, selectivity and formation rate of C_2 products, and/or to minimize the formation rate of CO_x products simultaneously. One must perform a systematic multi-objective optimization (MOO) study to determine the optimal operating conditions and design configurations of the SOFC unit.

Several two objective optimization problems were studied to find out the optimal conditions for the operation of an existing setup. Thereafter, a three objective optimization problem was also performed to have a better insight of all the solutions obtained in this study. Details of optimization formulations, bounds of the decision variables as well as values of other parameters used were given in Table 4. Upper and lower bound of these operating parameters were chosen based on the stability of the system as observed by Kiatkittipong et al. [8] and on the mathematical feasibility.

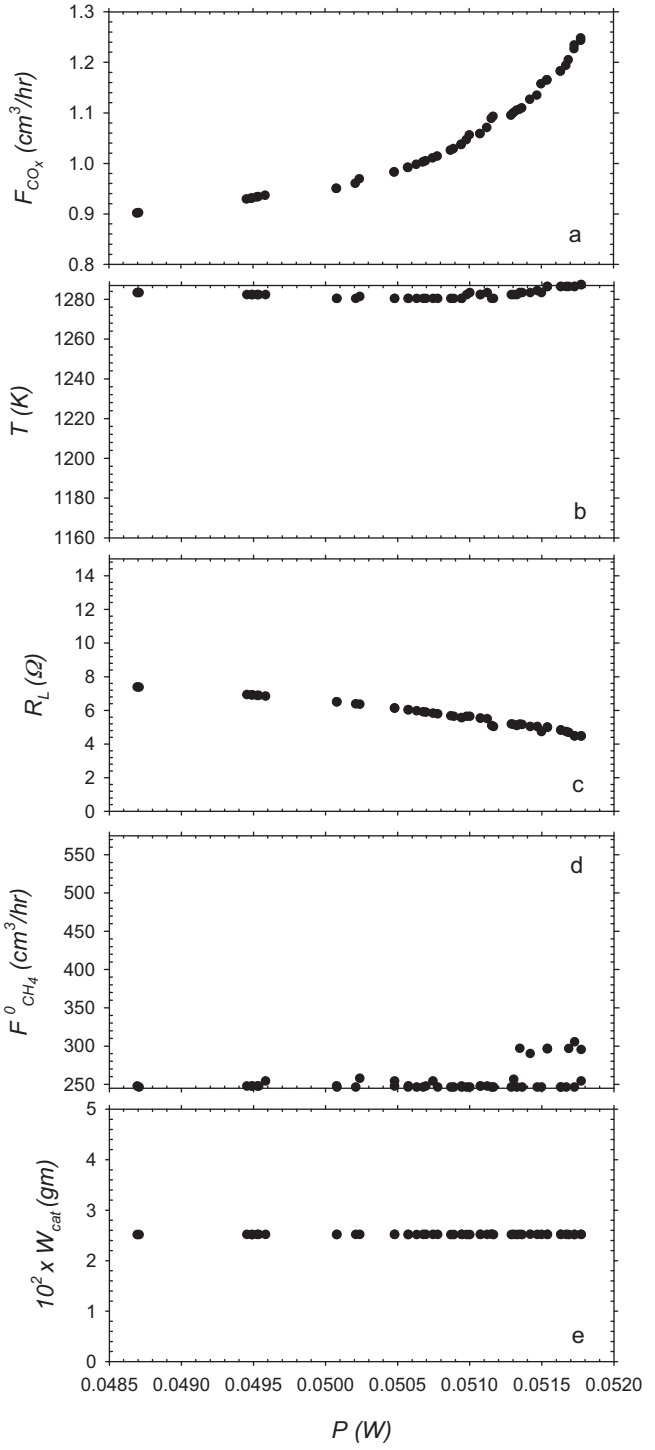

Fig. 5. Results of maximization of P and minimization of F_{CO_x}: (a) Pareto-optimal set; (b)–(d) values of decision variables corresponding to the points of Pareto-optimal set shown in part (a).

4. Results and discussion

Among the several available methods for solving the MOO problems, non-dominated sorting genetic algorithm (NSGA) has been widely used. NSGA differs from the simple GA only in the way the selection operator works [19]. NSGA uses a ranking selection method to emphasize the good chromosomes and niche method to create diversity in the population without losing a stable sub-population of good chromosomes. NSGA-II [20] is a further improvement of NSGA; it is an elitist NSGA using an elite-preservation strategy as well as an explicit diversity-preserving mechanism. By applying elitism better convergence near the true Pareto optimal front and better spread of Pareto optimal solutions was obtained, but resulted in decreased genetic diversity. Kasat and Gupta [21] introduced the concept of jumping genes in NSGA-II and the adaptation is referred as NSGA-II-JG. They applied NSGA-II-JG to optimize the same FCCU and showed that the adaptation was able to maintain genetic diversity while at the same time also reduces computation time. In this work, all the MOO problems were solved using NSGA-II-aJG [22], an improved version of NSGA-II.

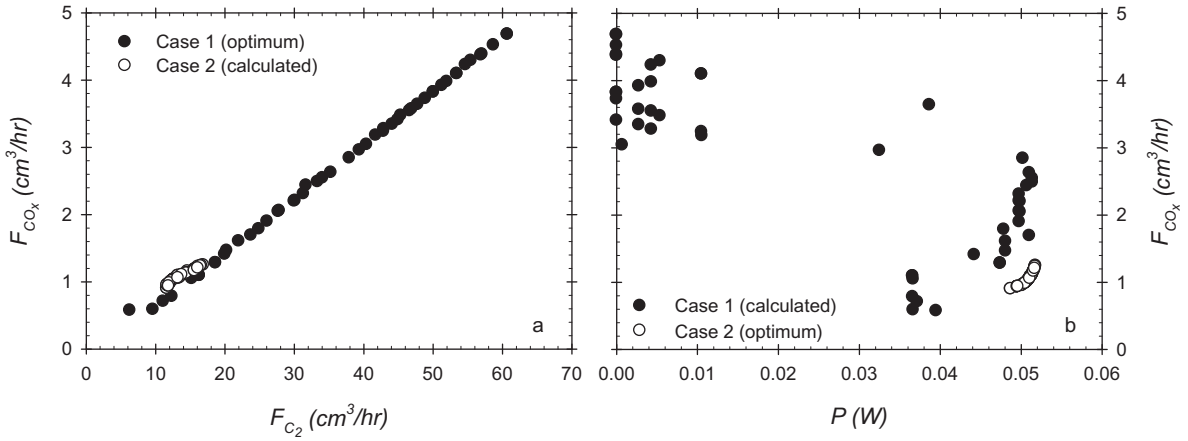

Fig. 6. Comparison of case 1 and case 2: (a) case 1 (optimum) and case 2 (calculated) and (b) case 1 (calculated) and case 2 (optimum).

The solution of multi-objective problems with conflicting variables give rise to Pareto-optimal set, which provides a spectrum of trade-offs between the competing objectives. In this section, the objective functions and corresponding decision variables were plotted, and compared with the corresponding reported experimental values. The results obtained were also explained qualitatively.

4.1. Case 1: maximization of C_2 flow (F_{C_2}) and minimization of CO_x flow (F_{CO_x})

Fig. 3(a) shows the Pareto-optimal set obtained for the simultaneous maximization of F_{C_2} and minimization of F_{CO_x} (case 1 in Table 4). A contradictory behavior is observed between the two objectives, i.e., moving from the left to the right (for example, from point C to F) the F_{C_2} increases at the cost of increased F_{CO_x}. Hence, each point on the Pareto set is equally good. The experimental results are also plotted in the same plot using open circle (◯) symbol. It is clearly evident that the Pareto points are far better than the existing operating points. Thus, the results provide the option to improve the performance of SOFC beyond the present operating condition. The maximum possible F_{C_2} (point F) is 60.71 cm^3/h accompanied by 4.68 cm^3/hr of CO_x exceeded the maximum experimental results of F_{C_2} (Point B) by 95% at the cost of slight increase (3.0 (point B) to 4.68 (point F) cm^3/h) of CO_x production. Besides, at the same generation of F_{CO_x} (point B), it is possible to produce more F_{C_2} (point E) at the cost of slight higher T and $F^0_{CH_4}$. Thus, the results obtained not only provide better results but also reveal the existence of greater flexibility at maneuvering the performance of SOFC.

Each point on the Pareto-optimal front corresponds to a set of decision variables, which are plotted in Fig. 3(b)–(e) against F_{C_2} to establish the fidelity of the results. The maximum and minimum values of y-axis in Fig. 3(b)–(e) represent the upper and lower bounds of the respective decision variables. From sensitivity analysis discussed earlier it was clear that both the objectives increased with increasing T. The percentage increase in F_{C_2} compared to the increase of F_{CO_x} was much larger. Hence it was expected that T to hit the upper bound. Similar behavior was also anticipated for $F^0_{CH_4}$. Although the percentage increase in this case was not much sensitive like T. Few scattered points in Fig. 3(e) are the consequence of this but still $F^0_{CH_4}$ was high enough compared to the operating points.

Increase in F_{C_2} and F_{CO_x} also resulted at low value of R_L. Thus, when simultaneous maximization of F_{C_2} and minimization of F_{CO_x} was considered, a smooth decrease in R_L form the highest value to the lowest was expected. It was quite obvious from Fig. 3(c) with an aberration that for the same value of resistance there was significant increase in both the objectives. Therefore, Fig. 3(e) where W_{cat} is plotted against F_{C_2}, it is considered to explicate the reasons behind the aberration. The plot was quite scattered with a repetitive pattern, hardly enlightened any explanation for the problem, rather put forward to consider the existence of degrees of freedom in selecting the combination of decision variables for certain points in the Pareto. In other words, more than one combination of these two decision variables could generate the same values of the objective functions. For example, any point on the Pareto could be generated by increasing R_L and W_{cat} or decreasing R_L and W_{cat} or any other combination of these two. Therefore, different combinations of R_L and/or W_{cat} might result in a set of identical objective function values. Moreover, insignificant influence of decision variables on the objective functions was also responsible for sparse data points.

In order to verify this further, the same problem (case 1) was carried out with fixing either R_L or W_{cat}. Fig. 4 presents the results obtained by fixing W_{cat} at its highest value. It was undoubtedly evident by the smooth trend of R_L that the degrees of freedom were eliminated successfully. So in conclusion, though it was possible to have a smooth trend by fixing some of the variables, the Pareto obtained in this case provided more flexibility to select an optimum point for efficient operation than the results reported by Kiatkittpong et al. [8] experimentally.

4.2. Case 2: maximization of power (P) and minimization of CO_x flow (F_{CO_x})

This case study was performed with some constraint on the overall conversion of the reactor. Sensitivity analysis portrayed that $F^0_{CH_4}$ and W_{cat} had no influence on the maximization of P. They were only related to the minimization of F_{CO_x}. As a result, to reach this objective, $F^0_{CH_4}$ will hit very high values, which reduce the retention time within the reactor and lead to low values of conversion. Thus, a constraint was put so that the solutions would be penalized if the conversion was below 10%. The results of simultaneous maximization of P and minimization of F_{CO_x} are presented in Fig. 5(a). The increase in P followed by the increase in F_{CO_x} revealed the contradictory behavior of the results. Every point on the Pareto denotes the maximum electrical power production possible at the minimum formation of CO_x. Moreover, it is apparent that slight increase in the CO_x production led to achieving higher values of P. Decision variables correspond to this Pareto set are plotted in Fig. 5(b)–(e).

The increase in both P and F_{CO_x} with the increasing T was observed in sensitivity analysis. But the temperature in this case

did not hit the upper bound like it did in case 1. In case 1 the effect of T on F_{C_2} was much higher than F_{CO_x} which was not obvious in case 2. P was found to be slight more sensitive than F_{CO_x} and as a result T reaches almost the highest bound and varied within the range of 1280–1287 K. The decision variable R_L was found to be the most important because of its direct relation with P. Moreover, the flow of oxygen to the anode side was controlled by varying R_L. As a result with the increasing values of P, R_L decreased and reached a lowest value of 4.5 Ω. This is due to decrease in the resistance of electron transfer, which allows more oxygen ion to permeate to the anode side and resulted in simultaneously increase in P for increasing electron flow and in the formation of CO_x for increased conversion. It was also reported by Kiatkittipong et al. [8] that the cell generated maximum power when the internal resistance of the cell equaled the R_L. The maximum power in this case was 0.0517 W and from the associating decision variable of this point the internal resistance was calculated using Eq. (A14). It was found that both R_{int} and R_L were equal to 4.5 Ω at this point. The power decreased beyond this point of R_L. This was also accompanied by an increasing in F_{CO_x} as more oxygen ion was allowed to permeate to the anode catalyst. Both these effects are against the objectives considered in this case and thus there is no R_L value lower than 4.5 Ω.

Other decision variables like $F^0_{CH_4}$ and W_{cat} showed the expected results. However, W_{cat} did not reach the lower bound in this case even though the bound was relaxed enough. This was mainly to maintain a high conversion of the feed gas.

Comparisons of the calculated and optimum results of both the cases are presented in Fig. 6. It is observed that optimum results of case 1 are better in terms of its objectives than those of case 2 and vice versa. In Fig. 6(a), at the same off gas generation, Case 1 produced more C_2 than case 2, whereas in Fig. 6(b) at the same power production, more off gases were generated in Case 1 than in case 2. So it could be concluded that both the Pareto sets were equally good in terms of their objectives.

4.3. Case 3: maximization of power (P) and C_2 flow (F_{C_2})

From Fig. 6(a), it is apparent that the maximum C_2 production in case 2 was very low (16.87 cm^3/h) where in case 1 it was 3.6 times higher (60.71 cm^3/h). So simultaneous maximization of F_{C_2} and P had drawn considerable attention because of its high economical value. Fig. 7(a) portrays the results of maximization of P and F_{C_2} at the same time. As expected a complementary behavior was observed, increase in P achieved at the cost of reduced production of C_2 products. However, the C_2 production in this case was doubled from Case 2. The maximum F_{C_2}, which was produced at the cost of zero power generation, resembled the value obtained in case 1.

The decision variables corresponds to the Pareto are plotted in Fig. 7(b)–(e). The values of R_L in this case never reached above 4.5 Ω. From the corresponding decision variable value of this point, calculation of R_{int} resulted a value close to 4.5 Ω. Thus, it authenticated the trend of R_L as it had already been discussed that maximum power could be achieved when R_{int} is equal to R_L. Besides, increasing value of R_L hindered the flow of electron, thus resulted in less conversion which in turn generated less C_2. The variation of other decision variables (T, $F^0_{CH_4}$ and W_{cat}) had already been discussed in detail and is similar to the previous analysis, thus any further explanation has not been included here.

4.4. Case 4: maximization of P and F_{C_2}, and minimization of F_{CO_x}

All the optimization studies discussed above illustrated that not all the three objectives could be improved at a time when only two objectives were considered, e.g., when maximization of P and F_{C_2} were considered, F_{C_2} was not optimum and, when maximization of P and minimization of F_{CO_x} were considered, F_{C_2} was also not optimum. Hence a three objective optimization, maximization of P and F_{C_2}, and minimization F_{CO_x}, is of interest for complete analysis and better understanding of the system performance.

The results in this case were shown in Fig. 8(a) and (b). In this figure, F_{C_2} and F_{CO_x} are plotted against P. The results obtained with different sets of values of computational parameters in NSGA-II-

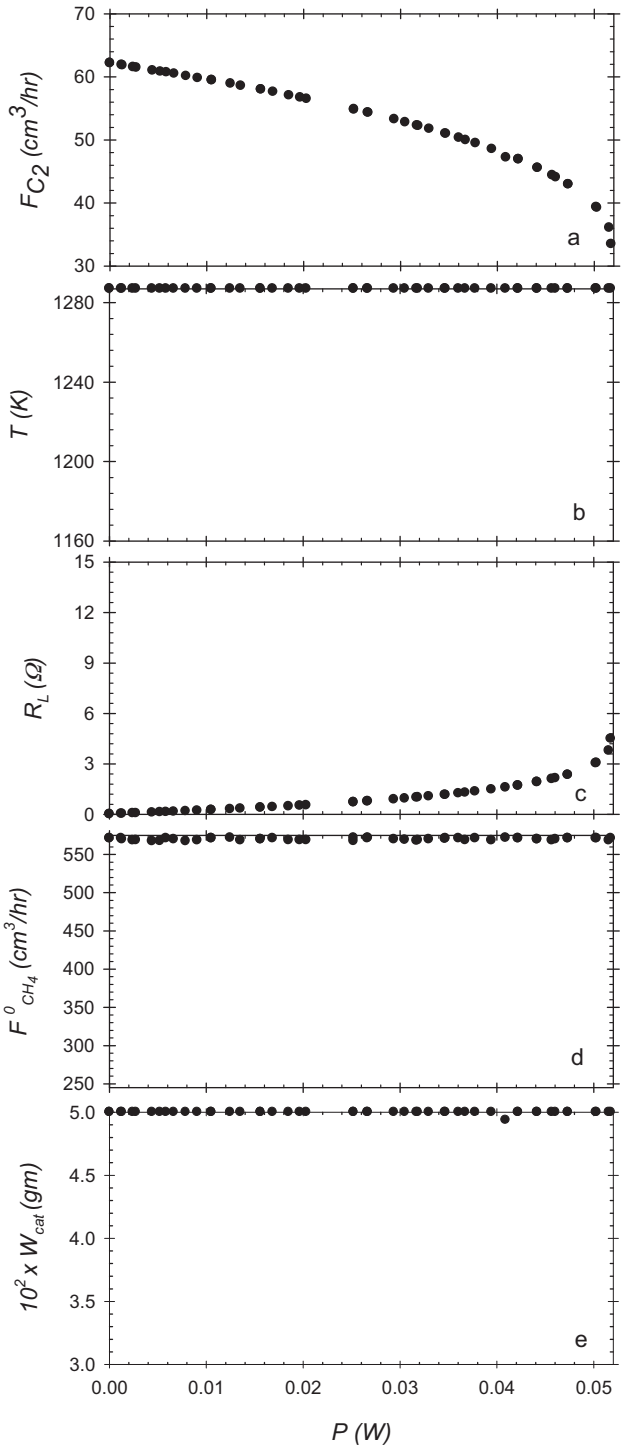

Fig. 7. Results of maximization of P and F_{C_2}: (a) Pareto-optimal set; (b–d) values of decision variables corresponding to the points of Pareto-optimal set shown in part (a).

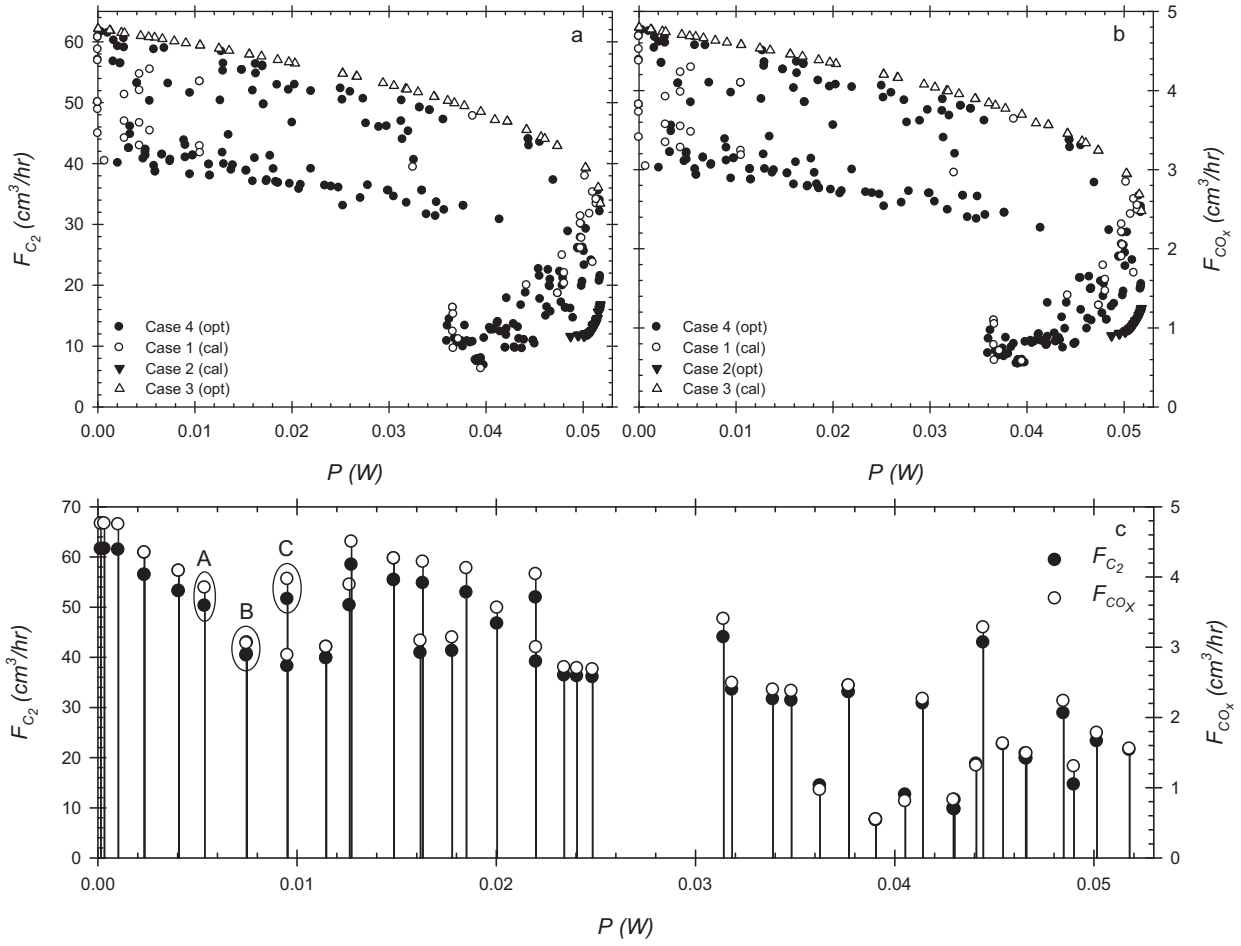

Fig. 8. Results of maximization of P and F_{C_2}, and minimization of F_{CO_x} (case 4).

aJG are also plotted on the same figure. The Pareto thus generated presents wide range of optimal values. Although the plots are visually scattered, all points are non-dominating i.e., moving from one point to another in the plot at least one objective function improves and at least another worsens. The scattered appearance is due to the fact that between two successive points either two objective function values improve (with one deteriorating) or one value improving while two others worsening. To establish the fidelity of the non-domination results of F_{C_2} and F_{CO_x} obtained with one set of NSGA-II-aJG parameter, the results are re-plotted against increasing P in the same figure (Fig. 8(c)). In Fig. 8(c), from point A to B, P increased (desired) and F_{CO_x} decreased (desired), but there is a decrease in F_{C_2} (undesired) meaning two objectives were improved while one deteriorated. Similarly, when moving from point B to C, both P and F_{C_2} improved (desired) but accompanied by undesired increase of F_{CO_x}. In this case also, two values improved while one deteriorated. However, there is no pair in Fig. 8(c), where all three objectives improved or worsened. Therefore, all points in Fig. 8(c) are equally good non-dominated solutions.

Three-objective optimization (case 4) results were compared with the results obtained from two-objective optimization (case 1, 2 and 3). For both the three and two-objective optimizations, F_{C_2} and F_{CO_x} are plotted against the P in Fig. 8(a) and (b). Note that, for the case 1, the values of P, for case 2 the values of F_{C_2} and for case 3 the values of F_{CO_x} corresponding to their Pareto front were calculated and shown in the same figure.

It was evident that the tradeoff between P and F_{CO_x} in case 2 (Fig. 8(b)) was better than the results obtained by three-objective optimization (case 4). However, the calculated values of F_{C_2} corresponds to Pareto front of case 2 was lower than in case 4 where F_{C_2} was simultaneously maximized (Fig. 8(a)). Again, the results of case 3 (Fig. 8(a)), where P and F_{C_2} was maximized simultaneously, was better than case 4, but the calculated results of F_{CO_x} for case 3 showed that the results were worse than case 4 in terms of minimization of F_{CO_x} (Fig. 8(b)). Similar results were also observed for case 1. At maximum F_{C_2} and minimum F_{CO_x}, though the P generated by this case had shown some high values of P, the results obtained for three-objective optimization had points where P was much higher than case 1. Moreover the diversity in the results obtained in case 4 was more than for case 1. Therefore, the Pareto for case 4 when all three objective functions are simultaneously optimized is better than any of three two-objective function optimization. This is due to the fulfillment of the criterion of domination by every point, i.e., attainment of any of the three objectives a sufficiently high value, despite simultaneous devaluation of the other two objectives. The reliability of the Pareto front in case 4 was also affirmed by the bounds generated from the results of two-objective.

The decision variables from the three-objective optimization are plotted in Fig. 9 against P to quantify the influence of decision variables on the objective functions as well as to authenticate the fidelity of the results obtained for case 4. It can be seen that the results are quite scattered and followed a wider range. The scattering of decision variables for three-objective were observed even when different sets of values for the computational parameters having been tried using NSGA-II-aJG. Similar reasons as discussed in case 1 lead to these scattered optimal solutions of the decision variables. These scattered optimal solutions imply the possibility of

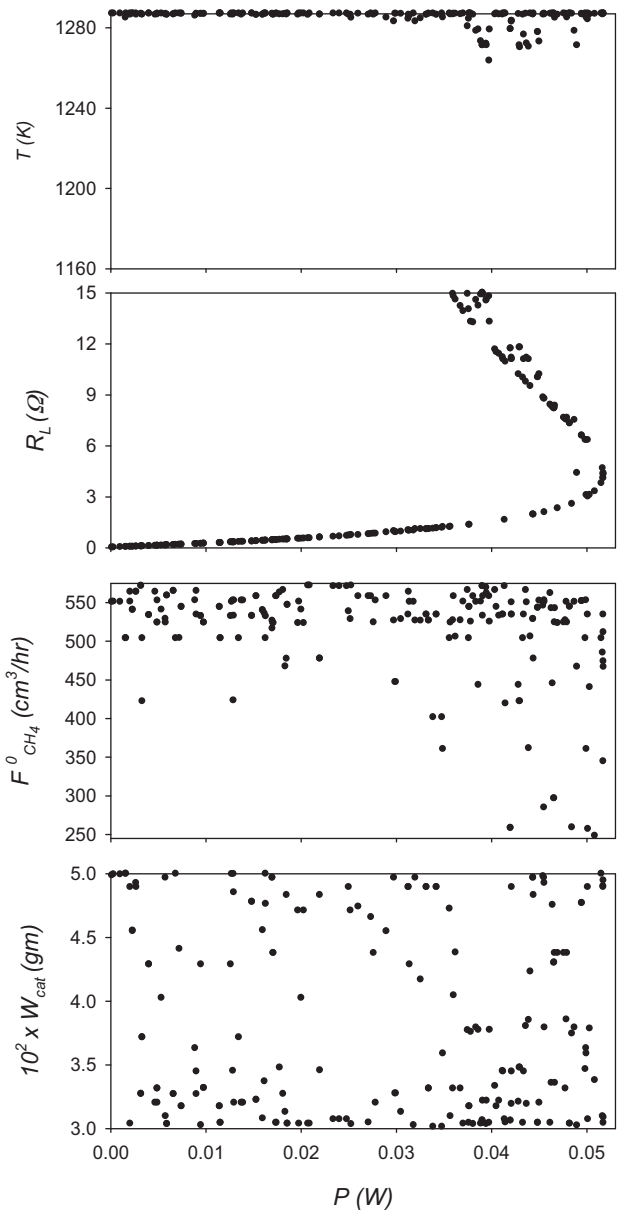

Fig. 9. Decision variables corresponding to the Pareto optimal solutions for case 4.

having degrees of freedom or multiplicity in selecting combination of decision variables for certain points in the Pareto.

5. Conclusions

Combination of several or many individual SOFC in a "stack" configuration results in formation of more valuable products and is particularly suited for combined heat and power generation because of elevated operating temperature. Modeling and optimization of SOFC has thus become a great tool to understand its performance. The single cell SOFC model developed by Kiatkittpong et al. [8] in this study was in good agreement with the experimental results and thus facilitated interfacing of the model with NSGA-II-aJG for multi-objective optimization study. Several two-objective and a three-objective optimization studies were performed on this model, all having high significance in important industrial and environmental issues. Formulations of all optimization problems were based on sensitivity analysis of the decision variables on the performance parameters of the SOFC unit. The results of simultaneous maximization of F_{C_2} and minimization of F_{CO_x} achieved 95% more C_2 production than present operating conditions at the cost of slight increase in CO_x production. This optimization brought out the presence of degrees of freedom within the system parameters which were not intuitive apparently. Maximization of electrical power and minimization of F_{CO_x} resulted in a decrease in F_{C_2} production whereas maximization of P and F_{C_2} was accompanied by more generation of F_{CO_x}. Both these outcomes were in contrast with the prime consideration of this study. As a result a three objective optimization where maximization of P and F_{C_2}, and minimization of F_{CO_x} was performed simultaneously. The results of this study provided better distributed and wider spread of optimal solutions to run the SOFC at desired level. All the trends of decision variables correspond to the optimal values of the objectives were possible to explain qualitatively and thus authenticated the reliability of the results.

Most importantly, this study extended the flexibility for a designer to choose the best optimal solutions and emphasized on the significance of multi-objective optimization with NSGA-II-aJG. The results would be worthwhile when more than one cell are coupled together for practical purposes, like SOFC stack.

Appendix A.

A.1. Reaction kinetics

When methane was fed on the anode and oxygen was permeated from the cathode to the anode side, the following oxidation reactions occurred:

$$CH_4 + (1/2)O_2 \rightarrow C_2H_6 + H_2O \quad (A1)$$

$$C_2H_6 + (1/2)O_2 \rightarrow C_2H_4 + H_2O \quad (A2)$$

$$CH_4 + (2/3)O_2 \rightarrow CO + 2H_2O \quad (A3)$$

$$CH_4 + 2O_2 \rightarrow CO_2 + H_2O \quad (A4)$$

$$C_2H_6 + (7/2)O_2 \rightarrow 2CO_2 + 3H_2O \quad (A5)$$

Then, the kinetic rate expressions determined for each of the above reactions (A1)–(A5) were given as follows, respectively.

$$r_1 = k_1 p_{CH_4} J_{O_2,cou} \quad (A6)$$

$$r_2 = k_2 p_{C_2H_6} J_{O_2,cou} \quad (A7)$$

$$r_3 = k_3 p_{CH_4} J_{O_2,oxy} \quad (A8)$$

$$r_4 = k_4 p_{CH_4} J_{O_2,oxy} \quad (A9)$$

$$r_5 = k_5 p_{C_2H_6} J_{O_2,oxy} \quad (A10)$$

The values of kinetic parameters in Eqs. (A6)–(A10) were reported by Kiatkittipong et al. [8] and showed in Table A1.

Table A1
Values of kinetic parameters.

Parameter[a] ($m^2\ kg^{-1}\ Pa^{-1}$)	Pre-exponential factor, A ($m^2\ kg^{-1}\ Pa^{-1}$)	Activation energy, E_a ($J\ mol^{-1}$)
k_1	3.70×10^7	215,000
k_2	2.96×10^5	110,000
k_3	4.14×10^2	124,000
k_4	2.96×10^2	131,000
k_5	1.78×10^5	120,000

[a] $k_i = A_i \exp(-E_{a,i}/RT)$.

A.2. Permeation in SOFC

The permeation of oxygen for a non-porous solid electrolyte was related to current (I) as described by Faraday's law as follow.

$$J_{O_2} = \frac{I}{4FA_sX} \tag{A11}$$

And the flux of oxygenate and coupling oxygen:

$$J_{O_2,cou} = y_{O_2,cou}J_{O_2} \tag{A12}$$

$$J_{O_2,oxy} = y_{O_2,oxy}J_{O_2} \tag{A13}$$

The overall setup can be presented as a simplified series circuit model, which consisted of a voltage source, E (SOFC reactor unit) with a variable external load resistor, R_L and internal resistance of the cell, R_{int}, which is the overall resistance including ohomic, activation and concentration polarization resistance inside the cell unit. Therefore, the R_{int} value varied with operating conditions such as temperature, total pressure of oxygen in the cathode (shell) side ($P_{O_2,CA}$) and was estimated experimentally. The following relation was used:

$$R_{int} = \frac{1.128 \times 10^{-2}}{P_{O_2,CA}^{0.2}T} \exp\left(\frac{166,000}{RT}\right) \tag{A14}$$

And for external load (R_L), the current (I) was calculated from

$$I = \frac{E}{R_{int} + R_L} \tag{A15}$$

This current was calculated using the experimental result of E at different R_L for different temperature (as reported in Fig. 8). The calculated current was used then to estimate the amount of oxygen permeated to the anode by Eq. (A11).

A.3. SOFC reactor model

The mass balance equation to the anode side is:

$$\frac{d\gamma_i}{dx} = \left[r_i + \left(\frac{A_s}{W_{cat}}\right)J_i\right]\frac{W_{cat}}{F_{CH_4}^0} \tag{A16}$$

Total pressure of oxygen in the cathode side (CA) was constant as pure oxygen was fed to the cathode and the partial pressure in the anode side (AN) was determined as follows:

$$p_{i.AN} = \frac{P_{t,AN}\gamma_i}{\sum \gamma_i} \tag{A17}$$

$$P_{O_2,CA} = 1.013 \times 10^5 \text{ Pa} \tag{A18}$$

CH_4 conversion (X_{CH_4}), C_2 selectivity (S_{C_2}) and power (P) of the SOFC unit, are calculated by:

$$X_{CH_4} = \frac{F_{CH_4}^0 - F_{CH_4}}{F_{CH_4}^0} \tag{A19}$$

$$S_{C_2} = \frac{2(F_{C_2H_6} + F_{C_2H_4})}{F_{CH_4}^0 - F_{CH_4}} \tag{A20}$$

$$P = I^2(R_L + R_{int}) \tag{A21}$$

References

[1] K. Otsuka, K. Jinno, Kinetic studies on partial oxidation of methane over samarium oxides, Inorg. Chim. Acta 121 (1986) 237–241.
[2] N. Pujare, A. Sammells, Methane activation to C_2 hydrocarbon species in solid oxide fuel cell, J. Electrochem. Soc. 02 (1988) 2544–2545.
[3] D. Eng, M. Stoukides, Catalytic and electrocatalytic methane oxidation with solid gxide membranes, Catal. Rev. 33 (1991) 375–412.
[4] S. Haile, Fuel cell materials and components, Acta Mater. 51 (2003) 5981–6000.
[5] A. Carrillo, T. Tagawa, S. Goto, Application of mist pyrolysis method to preparation of Ni/ZrO_2 anode catalyst for SOFC type reactor, Mater. Res. Bull. 36 (2001) 1017–1027.
[6] K.K. Moe, T. Tagawa, S. Goto, Preparation of electrode catalyst for SOFC reactor by ultrasonic mist pyrolysis—effect of spray time, J. Ceram. Soc. Jpn. 106 (1998) 754–758.
[7] K.K. Moe, T. Tagawa, S. Goto, Preparation of electrode catalyst for SOFC reactor by ultrasonic mist pyrolysis of aqueous solution, J. Ceram. Soc. Jpn. 106 (1998) 242–247.
[8] W. Kiatkittipong, T. Tagawa, S. Goto, S. Assabumrungrat, P. Paserthdam, Oxidative coupling of methane in the LSM/YSZ/LaAlO SOFC reactor, J. Chem. Eng. Jpn. 37 (2004) 1461–1470.
[9] W. Kiatkittipong, T. Tagawa, S. Goto, S. Assabumrungrat, P. Praserthdam, TPD study in LSM/YSZ/LaAlO system for the use of fuel cell type reactor, Solid State Ionics 166 (2004) 127–136.
[10] W. Kiatkittipong, S. Goto, T. Tagawa, S. Assabumrungrat, P. Paserthdam, Simulation of oxidative coupling of methane in solid oxide fuel cell type reactor for C_2 hydrocarbon and electricity co-generation, J. Chem. Eng. Jpn. 38 (2005) 841–848.
[11] T. Tagawa, K.K. Moe, T. Hiramatsu, S. Goto, Design of electrode for solid oxide fuel cells reactor, Solid State Ionics 106 (1998) 227–235.
[12] T. Tagawa, K.K. Moe, M. Ito, S. Goto, Fuel cell type reactor for chemicals-energy co-generation, Chem. Eng. Sci. 54 (1999) 1553–1557.
[13] T. Tagawa, K. Kuroyanagi, S. Goto, S. Assabumrungrat, P. Praserthdam, Selective oxidation of methane in an SOFC-type reactor: effect of applied potential, Chem. Eng. J. 93 (2003) 3–9.
[14] G. Xui-mei, K. Hidajat, C. Ching, Oxidative coupling of methane in a solid oxide membrane reactor, Ind. Eng. Chem. Res. (Anal. Ed.) 36 (1997) 3576–3582.
[15] G. Xui-mei, K. Hidajat, C. Ching, Simulation of a solid oxide fuel cell for oxidative coupling of methane, Catal. Today 50 (1999) 109–116.
[16] W. Kiatkittipong, T. Tagawa, S. Goto, S. Assabumrungrat, P. Praserthdam, Oxygen transport through LSM/YSZ/LaAlO system for use of fuel cell type reactor, Chem. Eng. J. 106 (2005) 35–42.
[17] D. Goldberg, Genetic Algorithms in Search, Optimization, and Machine Learning, Addison–Wesley, Reading, MA, 1989.
[18] K. Deb, Optimization for Engineering Design: Algorithms and Examples, Prentice Hall, New Delhi, 1995.
[19] V. Bhaskar, S.K. Gupta, A.K. Ray, Applications of multiobjective optimization in chemical engineering, Rev. Chem. Eng. 16 (2000) 1–54.
[20] N. Srinivas, K. Deb, Multi-objective function optimization using non-dominated sorting genetic algorithm, J. Evol. Comput. 2 (1995) 221.
[21] R.B. Kasat, S.K. Gupta, Multi-objective optimization of an industrial fluidized-bed catalytic cracking unit (FCCU) using genetic algorithm (GA) with the jumping genes operator, Comput. Chem. Eng. 27 (2003) 1785–1800.
[22] C. Guria, P.K. Bhattacharya, S.K. Gupta, Multi-objective optimization of reverse osmosis desalination units using different adaptations of the non-dominated sorting genetic algorithm (NSGA), Comput. Chem. Eng. 29 (2005) 1977–1995.